Journal of Solid State Chemistry 182 (2009) 1991–2003

Contents lists available at ScienceDirect

Journal of Solid State Chemistry

journal homepage: www.elsevier.com/locate/jssc

Phase diagram of the La–Si binary system under high pressure and the structures of superconducting $LaSi_5$ and $LaSi_{10}$

Shoji Yamanaka *, Satoshi Izumi, Shoichi Maekawa, Keita Umemoto

Department of Applied Chemistry, Graduate School of Engineering, Hiroshima University, Higashi-Hiroshima 739-8527, Japan

ARTICLE INFO

Article history:
Received 11 August 2008
Received in revised form
27 April 2009
Accepted 6 May 2009
Available online 15 May 2009

Keywords:
Lanthanum silicide
Crystal structure
Superconductor
High-pressure synthesis
Phase diagram
Electric band structure

ABSTRACT

The La–Si binary phase diagram under a high pressure of 13.5 GPa was experimentally constructed. New superconducting silicides $LaSi_5$ and $LaSi_{10}$ were found, which have peritectic decomposition temperatures at 1000 and 750 °C, respectively. The single crystal X-ray structural analysis revealed that there are two polymorphs in $LaSi_5$. The α-form obtained by heating a molar mixture of $LaSi_2$ and 3 Si at about 700 °C or by a rapid cooling from 1000 °C under pressure crystallizes with the space group $C2/m$ and the lattice parameters $a = 15.11(3)$, $b = 4.032(6)$, $c = 8.26(1)$ Å, and $\beta = 109.11(1)^\circ$. The β-form obtained by a slow cooling from 800–950 °C to 600 °C under pressure has the same space group but with slightly different lattice parameters, $a = 14.922(7)$, $b = 3.906(2)$, $c = 8.807(4)$ Å, and $\beta = 107.19(1)^\circ$. The β-form is formed during the incomplete transformation of the α-form on cooling, and has always been obtained as a mixture with the α-form. The compound can be characterized as a Zintl phase with a polyanionic framework $^3_\infty[Si_5]^{3-}$ with large tunnels running along the b axis hosting lanthanum ions. In the β-form, three of the five Si sites are disordered. The two polymorphs contain one dimensional sila-polyacene ribbons, Si ladder polymer, running along the b axis. The α-form showed superconductivity with the transition temperature T_c of 11.5 K. $LaSi_{10}$ crystallizes with the space group $6_3/mmc$ and the lattice parameters $a = 9.623(4)$, $c = 4.723(3)$ Å. It is composed of La containing Si_{18} polyhedra ($La@Si_{18}$) of hexagonal beer-barrel shape, which form straight columns by stacking along the c-axis via face sharing. One-dimensional columns of $La@Si_{18}$ barrels are edge-shared, and bundled with infinite Si trigonal bipyramid chains via corner sharing. The Si atoms in the straight chains have a five-fold coordination. $LaSi_{10}$ became a superconductor with $T_c = 6.7$ K. The *ab initio* calculation of the electric band structures showed that α-$LaSi_5$ and $LaSi_{10}$ are metallic, and the conduction electrons mainly come from Si-3p orbitals.

1. Introduction

Binary silicides with alkaline earth metals are pressure sensitive. The orthorhombic $BaSi_2$ undergoes the phase transition to the trigonal form at 5.2 GPa and 400 °C, and a trigonal to cubic transition at 600 °C [1–3]. The high-pressure trigonal and cubic forms adopt the $EuGe_2$ (or $CaSi_2$ like) and the $SrSi_2$ structures, respectively, which are corresponding to the structures of other alkaline earth metal disilicides with smaller atomic radii [3,4]. Binary silicides $SrSi_2$ and $CaSi_2$ are transformed to the α-$ThSi_2$ structures under pressures at elevated temperatures [5]. Binary compounds with the atomic ratios Si/Ba > 2 can be obtained only under high pressures at elevated temperatures. $Ba_{24}Si_{100}$ (Si/Ba = 4.17) was prepared under a pressure of 1.5 GPa at 800 °C [6] and Ba_8Si_{46} (Si/Ba = 5.75) under a pressure of 3.0 GPa at 800 °C [7]. These silicon-rich binary compounds belong to a silicon clathrate family; Ba_8Si_{46} is isotypic with Type I gas (G) hydrate $G_x(H_2O)_{46}$ [8], in which Ba containing silicon dodecahedra $Ba@Si_{20}$, and tetrakaidecahedra $Ba@Si_{24}$ are linked by face sharing to form the clathrate Si-sp^3 three dimensional network. Ba_8Si_{46} is a superconductor with a critical temperature (T_c) of 8.0 K. $Ba_{24}Si_{100}$ also consists of Ba containing silicon dodecahedral cages ($Ba@Si_{20}$), which are linked by sharing pentagonal faces to form a chiral zeolite-like network; the rest of the Ba atoms are located in the interstices of the network. Recently, it has been found that $Ba_{24}Si_{100}$ can also become a superconductor at $T_c = 1.4$ K [9].

A new Si-rich clathrate-like phase with a composition of $BaSi_6$ (Si/Ba = 6) has been synthesized under a much higher pressure of 12–15 GPa at 1000 °C [10], which is isomorphous with orthorhombic $EuGa_2Ge_4$ [11]; each Ba atom is surrounded by 18 Si atoms in an irregularly shaped polyhedron $@Si_{18}$. The polyhedra are connected by sharing faces to form Ba containing tunnels along a axis. Note that these Si-rich silicides (Si/Ba > 2) are obtained only under high pressure and high temperature conditions; the higher

* Corresponding author. Fax: +81 82 424 7740.
E-mail address: syamana@hiroshima-u.ac.jp (S. Yamanaka).

0022-4596/$ - see front matter © 2009 Elsevier Inc. All rights reserved.
doi:10.1016/j.jssc.2009.05.010

pressure used, the higher Si/Ba ratio obtained. Recently, isomorphous hexasilicides $SrSi_6$ [12] and $CaSi_6$ [13] were also prepared under high pressure. Similar high-pressure effects have been observed in the synthesis of Ge-rich compounds in the systems La–Ge [14] and Sr–Ge [15]. In this study, an attempt has been made of obtaining new Si-rich lanthanum silicides using a high pressure of 12–15 GPa range. In the La–Si binary system so far, only La_5Si_3 [16], La_3Si_2 [17], La_5Si_4 [18], LaSi [19,20], and $LaSi_2$ [4] with $Si/La \leq 2.0$ are known. The La–Si binary phase diagram has been constructed experimentally under a high pressure of 13.5 GPa, and new Si-rich phases $LaSi_5$ and $LaSi_{10}$ have been found.

2. Experimental

2.1. High pressure and high temperature experiment

$LaSi_2$ was prepared by an arc-melting under Ar atmosphere. High pressure and high temperature syntheses were carried out using Kawai-type multianvils [21]. The cell assembly and synthesis procedures were very similar to those used in $BaSi_6$ synthesis [10]. The intimate mixtures of $LaSi_2$ and Si powders under 100 mesh were filled in a cylindrical *h*-BN cell with an inner diameter of 2 mm, which was surrounded by a graphite tube heater. The heater was in turn surrounded by a calcium stabilized ZrO_2 tube for thermal insulation. The whole sample assembly was centered in a pierced CoO doped MgO octahedron with an edge length of 12 mm, which was placed in the center of eight truncated tungsten carbide cubes as anvils (truncation edge length: 6 mm) separated by pyrophyllite gaskets, and compressed in a multianvil apparatus up to 13.5 GPa. The sample in the *h*-BN cell was heated by resistive heating of the graphite tube. The temperature of the sample was monitored and controlled by a thermocouple on the *h*-BN cell. Various heating and cooling protocols were used to construct the phase diagram and to obtain single crystals. The La–Si binary system is reactive with *h*-BN cell at temperatures above 1000 °C. It was very difficult to keep the system at higher temperatures for more than 30 min. We sometimes used a Ta metal heater with a thickness of 0.05 mm instead of a thick graphite tube heater with a thickness of 0.75 mm to earn a much larger sample volume. However, the metal heater surrounding the outer side of an *h*-BN cell changed into $TaSi_2$ in a short time at temperatures above 1000 °C by the reaction with the binary system, and could not keep the electric current necessary for heating.

2.2. Characterization

Single crystal X-ray structural analysis was performed on a Rigaku AFC7R Mercury CCD diffractometer with Mo$K\alpha$ radiation ($\lambda = 0.71073$ Å) coupled with CrystalClear interface (Rigaku) for data collection, containing TwinSolve software for twined structure analysis. The single crystal structure was refined with the program SHELX97 [22] and the WinGX software package [23]. Powder X-ray diffraction (XRD) patterns were measured by an imaging plate Guinier diffractometer (Huber 670G) using Mo$K\alpha$1 (0.709260 Å) radiation and a glass capillary goniometer. The angular resolution FWHM (full width at half maximum) of the diffractometer was found to be ~0.12° in 2θ in the range of 20°–40° for LaB_6 standard. Cu$K\alpha$1 radiation was also used, but only a very weak diffraction signal was observed due to the strong X-ray absorption of the samples in the transmission diffraction mode. TOPAS-Academic software package was used for the Rietveld analysis [24]. The silicide composition was determined by a scanning electron microscope (SEM, Hitachi-3400) equipped with an energy dispersive X-ray microanalyser (EDX, EDAX Genesis XM2), using LaB_6 and Si as standards for La and Si contents. Magnetic susceptibilities were measured using a SQUID magnetometer (Quantum Design MPMS-5) under a field of 20 Oe. The electrical conductivity was measured by a standard four-probe technique down to 8.5 K with a Lakeshore ac resistance bridge (Model 370) and a Niki-Glass refrigerator (LTS-2005-TU). The *ab initio* calculations of geometry optimization, the density of states, and band structure were performed within the density functional theory (DFT) framework, using the program CASTEP [25,26] in Accelrys software suit. The calculations were carried out using the GGA-PBE (general gradient approximation, Perduw–Burke–Ernzehof) functional. Ultrasoft pseudopotentials were used within a plane wave basis with cut off energy of 270 eV.

3. Results and discussion

3.1. Phase diagram of the La–Si binary system under high pressure

$LaSi_2$ did not react with excess Si under a pressure below 8 GPa at 1000 °C. At 13.5 GPa and 1000 °C, new Si-rich binary phases $LaSi_5$, and $LaSi_{10}$ were obtained. The La–Si binary phase diagram showing the formation regions of the new Si-rich compounds was constructed by performing high-pressure and high-temperature treatments of $LaSi_2$ and Si mixtures in various ratios in different thermal protocols. The compositions of the grains and domains were determined using EDX under SEM. The La–Si binary phase diagram constructed based on the analytical data is shown in Fig. 1. Typical compositional images observed using reflection electrons of SEM, together with chemical compositional data of some test points are collected in Fig. 2. In the phase diagram the marked points with the sample numbers show the starting temperatures for rapid (triangle) and slow (open circles) coolings. The $LaSi_2$ and Si mixtures were heated for 1 h at the

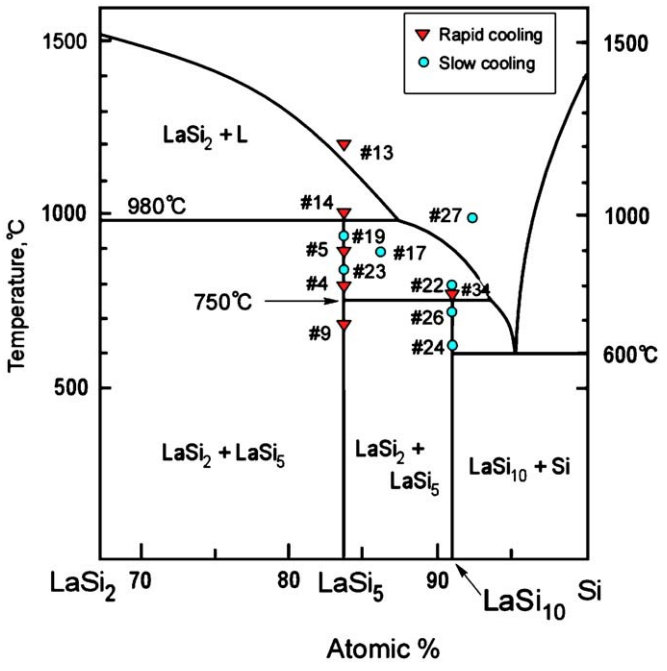

Fig. 1. Phase diagram of the La–Si binary system in the Si-rich region under a pressure of 13.5 GPa, constructed by the investigation of the samples prepared using rapid cooling (triangle) and slow cooling (open circle) process. Some of the SEM images of the numbered samples are given in Fig. 2 with the EDX analytical data.

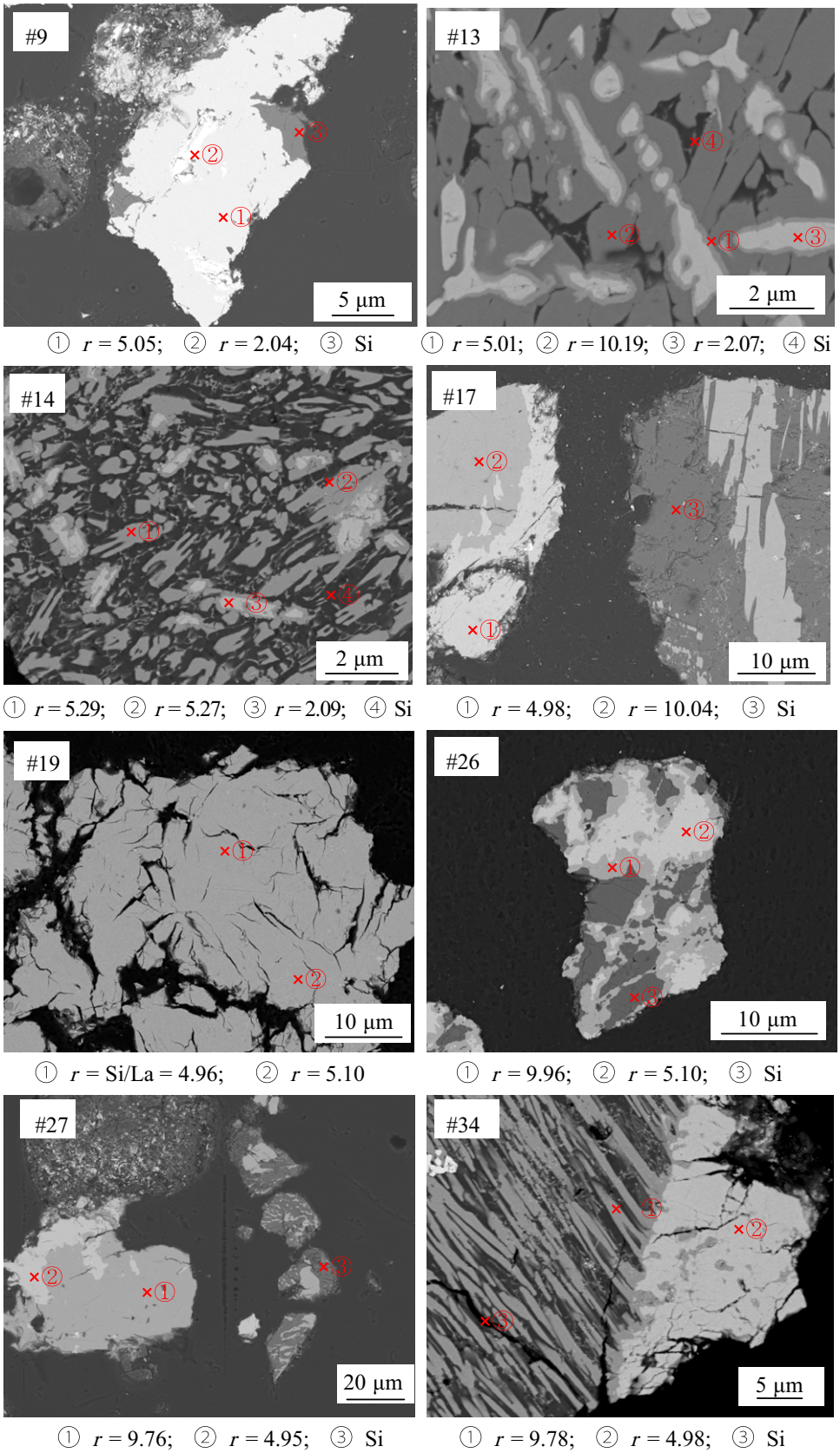

Fig. 2. Typical SEM compositional images of the samples marked in the phase diagram of Fig. 1. The EDX analytical data marked by numbers in each image are given, where "*r*" is an atomic ratio Si/La.

respective starting temperatures under 13.5 GPa, and cooled down for a rate of 100 °C/h for the slow cooling process unless other wise specified. The rapid cooling was performed down to 600 °C from the starting temperature within about 20 s under pressure. The pressure was released gradually after the temperature returned to room temperature.

The melting temperatures of $LaSi_2$ (1520 °C) and Si (1410 °C) in the phase diagram are tentatively taken from references for ambient pressure [27,28]. $LaSi_5$ and $LaSi_{10}$ were found to be compounds with peritectic temperatures at about 980 and 750 °C, respectively. The following samples analyzed by EDX are important to construct the phase diagram;

(1) Samples with nominal compositions Si/La = 5/1 (#4, #5, #9, #19, #23) heated at temperatures below 950 °C form a single phase with a composition La/Si = 5, irrespective of the cooling protocols. The grain sizes are grown to a dimension larger than 100 μm.

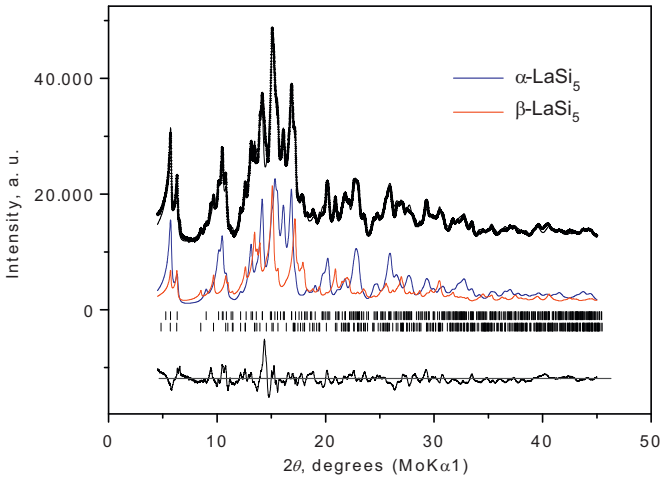

Fig. 3. Simulation fitting of the X-ray diffraction patter of the $LaSi_5$ sample (#4) prepared by rapid cooling from 800 °C. Open circles show the observed data points, solid lines represent the calculated diffraction patterns of total (black) and the two constituents (colors). The difference profile plot is shown at the bottom. The vertical bars represent the calculated reflection positions; α-$LaSi_5$ (top tick marks) and β-$LaSi_5$ (bottom tick marks). In the simulation, the lattice parameters and the atomic coordinates of Tables 1 and 2 were used. Only the scale factors and profile functions were refined. (For interpretation of the references to color in this figure legend the reader is referred to the web version of this article.)

(2) Sample #14 (Si/La = 5/1) was heated up to 1000 °C for 30 min, and rapidly cooled down to 600 °C. The product was a mixture of $LaSi_2$ and $LaSi_5$+Si, the domain sizes being smaller than 10 μm.

(3) Sample #13 (Si/La = 5/1) was heated up to 1200 °C for 30 min, and then rapidly cooled down to 600 °C. Small $LaSi_2$ cores (< 1 μm in diameter) are covered by thin $LaSi_5$ layers, which are in turn surrounded by a $LaSi_{10}$ phase. Silicon is located in the interstices of the $LaSi_{10}$ grains.

(4) Samples #24 and #26 (Si/La = 10/1) were heated to temperatures below 750 °C as shown in Fig. 1, and then slowly cooled down to 500 °C. The product is composed of $LaSi_{10}$ and $LaSi_5$ and Si. The $LaSi_{10}$ phase is grown between $LaSi_5$ and Si grains. Note that although the reaction temperature is relatively low, there is no starting $LaSi_2$ phase left unreacted in the product. This suggests that $LaSi_2$ reacts with Si to form $LaSi_5$ in the first reaction stage, and then $LaSi_{10}$ is formed by the reaction of $LaSi_5$ and Si.

(5) Sample #22 (Si/La = 10/1) is heated up to 800 °C, and slowly cooled down to 600 °C. The product is mainly a mixture of $LaSi_5$ and $LaSi_{10}$ with Si. $LaSi_5$ and $LaSi_{10}$ domains are grown to about 40 μm in diameter.

(6) Sample #34 (Si/La = 10/1) is heated up to 780 °C, and rapidly cooled down to 600 °C. The product mainly consists of a mixture of fine domains of $LaSi_{10}$ and Si with relatively large grains of $LaSi_5$.

(7) Sample #17 (Si/La = 6/1) was heated at 800 °C, and then slowly cooled down to 600 °C. The product is a mixture of $LaSi_5$ and $LaSi_{10}$ with Si. The grains were grown to a dimension larger than 20 μm.

(8) Sample #27 (Si/La = 12/1) was heated at 1000 °C, and then slowly cooled down to 600 °C. The product is composed of $LaSi_5$ and $LaSi_{10}$ with Si. $LaSi_{10}$ crystals larger than 50 μm were found.

Table 1
Details of the crystal structure investigations for α-, β-$LaSi_5$, and $LaSi_{10}$.

	α (Rapidly cooled form)	β (Slowly cooled form)	$LaSi_{10}$
Formula	$LaSi_5$	$LaSi_5$	$LaSi_{10}$
Formula weight	279.36	279.36	419.81
Crystal size (mm)	0.05 0.05 0.02	0.05 0.05 0.03	0.05 0.05 0.02
Space group	*C*2/*m*	*C*2/*m*	$P6_3/mmc$
A (Å)	15.11(3)	14.922(7)	9.623(4)
B (Å)	4.032(6)	3.906(2)	9.623(4)
c (Å)	8.263 (13)	8.807(4)	4.723(3)
β (°)	109.111(16)	107.19(1)	(*γ* = 120)
V (Å^3), *Z*	475.7(14), 4	490.4(4), 4	378.8(3), 2
d_{calc} (g/cm^3)	3.901	3.784	3.681
Temperature, K	293	293	293
λMoKα (Å)		0.71073	
μ (mm^{-1})	10.049	9.747	7.128
Absorption correction	Empirical	Numerical	Empirical
F(000)	508	508	394
θ_{max}		27.48	
Index ranges	$-9<h<18$, $-4<k<5$, $-10<l<9$	$-17<h<19$, $-5<k<4$, $-11<l<9$	$-9<h<12$, $-12<k<9$, $-4<l<6$
Total reflections	1592	1882	2696
Unique reflections	551	632	187
Mosaicity (°)	3.73	2.14	2.55
R_{int}	0.056	0.015	0.0754
Observed [$I \geq 2\sigma(I)$]	522	631	184
No. of variables	38	62	18
GOF on Fo^2	1.092	1.305	1.344
R1/*wR2* [$I \geq 2\sigma(I)$]	0.0709/0.159	0.0558/0.1665	0.0682/0.1998
R1/*wR2* (all data)	0.0739/0.1607	0.0588/0.1665	0.0683/0.1999
Largest diff. peak and hole (e$^-$/Å^3)	3.157, −2.181	4.847, −2.913[a]	2.857, −2.405

[a] The largest difference peak (4.847 e) is located between Si1–La (1.22 Å from Si1 and 2.2 Å from La).

Taking the above observations into account, the peritectic temperatures of $LaSi_5$ and $LaSi_{10}$ were estimated to be 980 and 750 °C, respectively. The eutectic temperature of $LaSi_{10}$ and Si was tentatively located at 600 °C. For more precise phase diagram, the samples should be reground and re-heated at the same conditions. Nevertheless, the present phase diagram is helpful to understand the formation regions of $LaSi_5$ and $LaSi_{10}$ and their thermal properties.

3.2. Structural characterization and superconductivity of $LaSi_5$

Samples #4 (Si/La = 5/1) and #5 (Si/La = 5/1) were prepared by heating a molar mixture of $LaSi_2$ and 3 Si at 800 and 900 °C, respectively, for 1 h, followed by rapid cooling to 600 °C. Both samples gave a broad and complicated XRD pattern as shown in Fig. 3 for sample #4. As mentioned in Experimental, the angular resolution FWHM of the Guinier diffractometer used was better than ~0.12° in 2θ. The broad diffraction pattern indicates the poor crystallinity of the sample. Although the pattern was very broad, fortunately we could find several small crystals suitable for single crystal analyses in the products. There are two different types of crystals having the same composition $LaSi_5$, which will be hereafter called α- and β-$LaSi_5$. X-ray single crystal analyses were successfully performed, and the crystallographic data are listed in Table 1 and 2. Some selected bond distances are given in Table 3. The CCD image data collected on the single crystal of the disordered form β-$LaSi_5$, were analyzed by using TwinSolve program of CrystalClear (Rigaku). The program did not suggest the presence of any twin component. As shown in Fig. 3, the XRD simulation using TOPAS academic software on the mixture of the two types of polymorphs can reproduce the observed pattern of sample #4, where only the scale parameters and the peak profiles were refined using the lattice parameters and atomic coordinates determined by the respective single crystal analyses in Tables 1 and 2. The simulation revealed that sample #4 is a mixture of 64% of α- and 36% of β-$LaSi_5$. The mosaicities of the two types of $LaSi_5$ single crystals were determined in the refinement of the lattice parameters, and are given in Table 1. About 65 and 87% of the total data collected were accepted for α- and β-$LaSi_5$ single crystals, respectively. Note that the powder diffraction pattern of Fig. 3 is much broader than that expected from the mosaicities of the constituent single crystals. It is very likely that the single crystals represent the extreme end members of the α- and β-forms. The matrix from which the two types of single crystals were found can be a mixture of more-or-less poor crytalline α-like and β-like structures, and the averaging of mixed domains should be considered. The large mosaicity value of the α-form may also suggest a similar averaging effect of mixed domains.

Sample #9 (Si/La = 5/1) was prepared by heating a molar mixture ($LaSi_2$+3Si) at 700 °C for 1 h, and then rapidly cooled down to 600 °C. The product mainly consisted of α-$LaSi_5$. The lattice parameters were determined to be $a = 15.19(2)$, $b = 4.01(5)$, $c = 8.20(6)$ Å, and $\beta = 109.44(6)^\circ$ based on the powder XRD data. The parameters are in good agreement with

Table 3
Selected bond distances (Å) and angles (°) of α- and β-$LaSi_5$.

α-$LaSi_5$		β-$LaSi_5$	
Si5		Si5a	
|	2.368(10)	|	2.38(3)
Si4		Si4b	
|	2.383(6)	|	2.374(16)
Si3		Si3b	
|	2.306(16)	|	2.331(19)
Si3		Si3a	
|	2.383(6)	|	2.361(14)
Si4		Si4a	
|	2.368(10)	|	2.36(4)
Si5		Si5b	
Si1–Si1	2.424(8)	Si1–Si1	2.381(7)
Si1–Si4	2.324(9)	Si1–Si4a	2.304(14)
Si2–Si2	2.412(14)	Si1–Si4b	2.364(15)
Si2–Si5	2.484(6)	Si2–Si2	2.391(13)
		Si2–Si5a	2.374(10)
		Si2–Si5b	2.599(19)
La–Si1	3.093(6)	La–Si1	3.100(5)
La–Si1	3.263(8)	La–Si2	3.150(5)
La–Si2	3.181(6)	La–Si2	3.221(5)
La–Si2	3.237(7)	La–Si3a	3.106(10)
La–Si3	3.139(7)	La–Si3b	3.162(10)
La–Si4	3.352(9)	La–Si4b	3.281(14)
La–Si4	3.371(9)	La–Si5a	3.39 (3)
La–Si5	3.156(8)	La–Si5b	3.117(14)
Ave(La–Si)	3.224(7)	Ave(La–Si)	3.191(8)

Table 2
Atomic coordinates, site occupation factors (SOF), anisotropic and equivalent displacement parameters (Å^2) for α- and β-$LaSi_5$.

Atom	Position	SOF	x	y	z	U_{11}	U_{22}	U_{33}	U_{12}	U_{13}	U_{23}	Ueq
α-$LaSi_5$ (rapidly cooled form)												
La	4*i*	1	0.43191(10)	0	−0.27774(18)	0.0259(9)	0.0183(9)	0.0323(10)	0	0.0109(6)	0	0.025(6)
Si1	4*i*	1	0.2308(4)	0	0.4142(8)	0.020(3)	0.015(3)	0.033(3)	0	0.015(3)	0	0.021(2)
Si2	4*i*	1	0.4256(4)	1/2	0.0248(9)	0.022(3)	0.013(3)	0.038(4)	0	0.011(3)	0	0.024(2)
Si3	4*i*	1	0.4353(5)	1/2	0.3777(10)	0.029(3)	0.013(3)	0.053(5)	0	0.016(3)	0	0.031(2)
Si4	4*i*	1	0.3487(4)	0	0.2907(9)	0.026(3)	0.019(3)	0.030(3)	0	0.014(3)	0	0.024 (2)
Si5	4*i*	1	0.3253(4)	0	−0.0070(9)	0.023(3)	0.021(3)	0.032(4)	0	0.016(3)	0	0.024(2)
β-$LaSi_5$ (slowly cooled form)												
La	4*i*	1	0.42338(9)	0	−0.25712(15)	0.0085(7)	0.0093(7)	0.0089(7)	0	0.0003(4)	0	0.0094(4)
Si1	4*i*	1	0.2379(4)	0	0.4191(7)	0.009(3)	0.011(3)	0.009(3)	0	0.004(2)	0	0.0094(2)
Si2	4*i*	1	0.4254(5)	1/2	0.0245(8)	0.019(3)	0.012(3)	0.012(3)	0	0.005(2)	0	0.015(2)
Si3a	4*i*	0.5(5)	0.4287(9)	1/2	0.3168(16)	0.010(6)	0.008(6)	0.016(8)	0	0.006(5)	0	0.011(4)
Si3b	4*i*	0.5(5)	0.469(1)	1/2	0.4255(15)	0.020(7)	0.009(6)	0.009(8)	0	0.007(6)	0	0.012(5)
Si4a	4*i*	0.50(5)	0.3358(14)	0	0.260(3)	0.011(9)	0.010(6)	0.010(11)	0	0.004(9)	0	0.010(6)
Si4b	4*i*	0.50(5)	0.3771(15)	0	0.343(3)	0.014(10)	0.010(7)	0.018(13)	0	0.013(10)	0	0.012(7)
Si5a	4*i*	0.47(6)	0.3437(17)	0	0.061(3)	0.013(10)	0.010(7)	0.006(12)	0	−0.001(10)	0	0.011(7)
Si5b	4*i*	0.53(6)	0.306(2)	0	−0.018(4)	0.025(13)	0.026(8)	0.023(16)	0	0.019(13)	0	0.022(8)
Si3[a]	4*i*	1	0.449	1/2	0.371							
Si4[a]	4*i*	1	0.356	0	0.302							
Si5[a]	4*i*	1	0.325	0	0.021							

Note: U_{eq} is defined as one third of the trace of the orthogonalized U tensor.

[a] Averaged coordinates between the disordered sites.

those given in Table 1 for α-$LaSi_5$. The samples obtained after heating at temperatures above 800 °C such as #4, #5, #19, and #23 are mixtures of α- and β-$LaSi_5$, irrespective of the different heating and cooling protocols used. The samples obtained by a rapid cooling from sufficiently high temperatures above 1000 °C, #13 and #14, contained α-$LaSi_5$, $LaSi_2$ and other phases. It is strange that the same α-form was obtained from sample #9 prepared at a temperature as low as 700 °C. Note that the β-form was obtained only by heating the sample to temperatures above 800 °C followed by a slow or a rapid cooling process, and that it was always accompanied by the α-form. It will be reasonable to characterize α- and β-$LaSi_5$ as rapidly and slowly cooled forms, respectively. The transformation of the α-form to the β-form appears to be very slow. $LaSi_5$ is a metastable high-pressure phase, which was found to decompose into $LaSi_2$ and Si on heating at 600 °C in vacuum or Ar atmosphere. For the synthesis of $LaSi_5$ a high pressure condition at least higher than 8 GPa was required at elevated temperatures.

The two polymorphs of $LaSi_5$ can be distinguished by the superconductivity. Sample #9 (α-$LaSi_5$) showed a sharp superconducting transition at $T_c = 11.5$ K as shown in Fig. 4 (a). The superconducting volume fraction was estimated to be more than

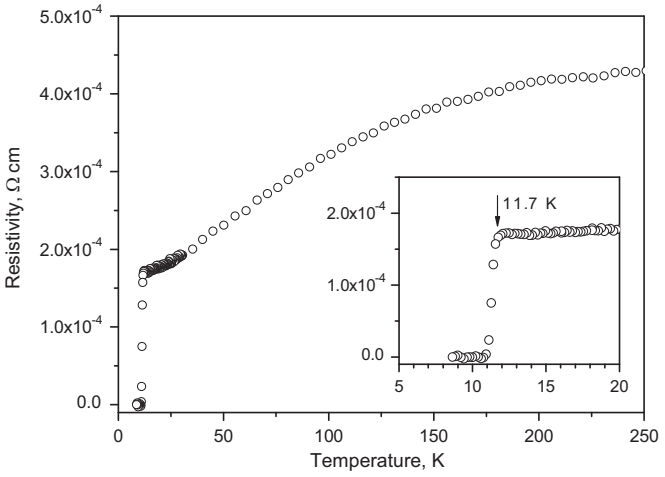

Fig. 5. Electrical resistivity as a function of temperature on α-$LaSi_5$ obtained by a rapid cooling. The inset shows the resistivity in the low temperature range.

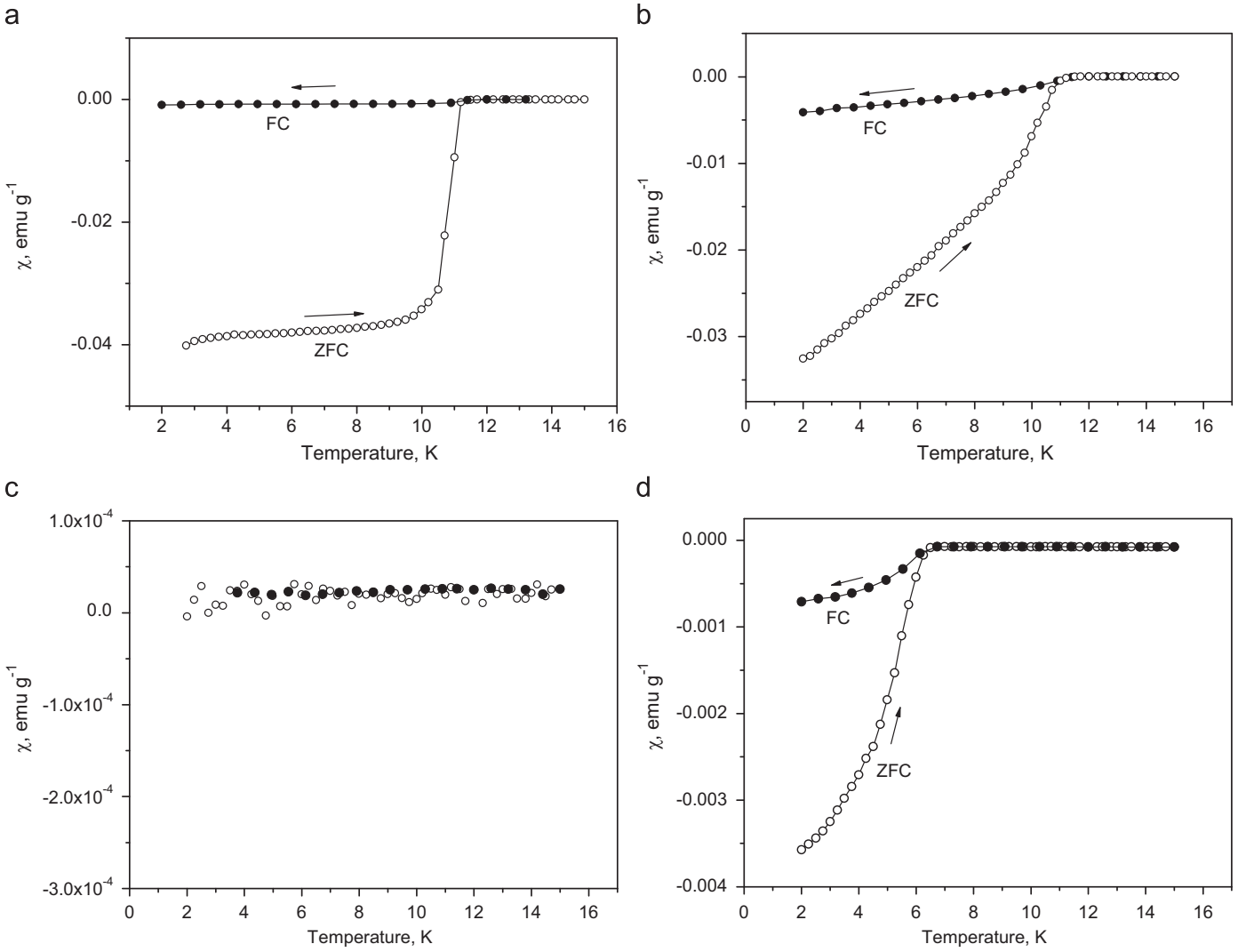

Fig. 4. Magnetic susceptibility curves as a function of temperature in zero-field-cooling (ZFC) and field-cooling (FC) modes on the $LaSi_5$ and $LaSi_{10}$ samples obtained using different heating and cooling protocols under pressure; (a) sample #9 (α-$LaSi_5$), (b) sample #33 (mixture of α- and β-$LaSi_5$), (c) β-$LaSi_5$ (single crystals from sample #4), and (d) $LaSi_{10}$.

100% from the diamagnetic susceptibility. Fig. 4 (b) shows the magnetic susceptibility of sample #33 (rapidly cooled down from 900 °C) as a function of temperature. The superconducting onset was observed at $T_c = 11.5$ K, the same T_c found for sample #9 (Fig. 4 (a)); the magnetic susceptibility gradually decreased down to 2 K. We have not yet succeeded in preparing β-$LaSi_5$ as a single phase. It is always obtained as a mixture with α-$LaSi_5$. Single crystals of β-$LaSi_5$ were picked up from samples #4 and #5, and identified by measuring the lattice parameters for each crystal using a single crystal diffractometer. The magnetic susceptibilities of several β-$LaSi_5$ single crystals were measured as a function of temperature. As shown in Fig. 4 (c), β-$LaSi_5$ was found to be Pauli-paramagnetic, and did not show a superconducting transition down to 2 K. This finding suggests that the magnetic susceptibility observed on the mixture of α- and β-$LaSi_5$ is ascribed to the contribution of the superconductivity of the α-form. The broad temperature dependence of the superconducting transition in the magnetic susceptibility curve of α-$LaSi_5$ could be due to the poor crystallinity corresponding to the broad XRD pattern of Fig. 3. The α-$LaSi_5$ sample obtained by a rapid cooling from 1000 °C showed the temperature dependence of the magnetic susceptibility similar to that shown in Fig. 4(a). The superconductivity of α-$LaSi_5$ appears to be sensitive to the crystallinity. $LaSi_2$ is also a superconductor with $T_c = 2.5$ K [29,30], and the contamination with $LaSi_2$ exhibits a small drop of the magnetic susceptibility at the corresponding temperature. The electrical resistivity was measured as a function of temperature on the sample rapidly cooled from 950 °C, and the result is shown in Fig. 5. The resistivity decreased with the decrease of temperature, and showed a steep drop at $T_c = 11.7$ K. The zero resistivity was attained at 10.7 K. The transition temperature in the electrical resistivity was in good agreement with that found for α-$LaSi_5$ by the magnetic susceptibility measurement.

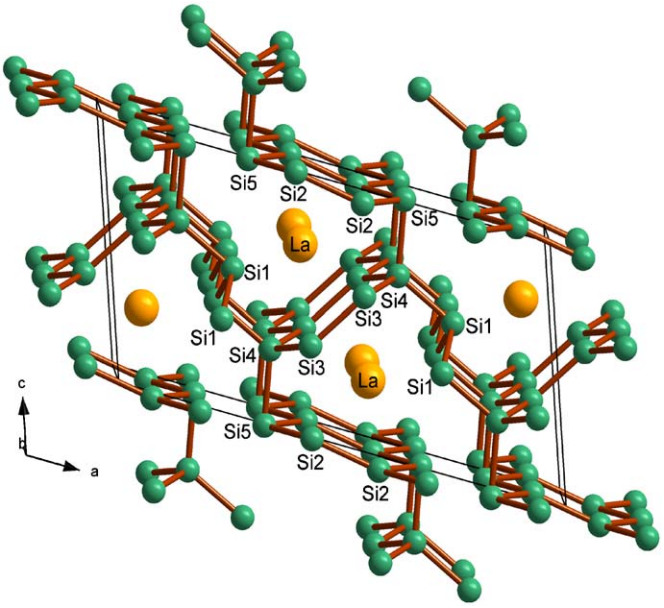

Fig. 6. Schematic illustration of the crystal structure of α−$LaSi_5$

Two types of $LaSi_5$ polymorphs crystallize with the same space group *C2/m*. The structures are schematically shown in Figs. 6 and 7 for the α- and β-forms, respectively. The crystals can be classified as Zintl compounds containing polyanionic frameworks ${}^{3}_{\infty}[Si_5]^{3-}$ with large tunnels running along the *b* axis hosting La^{3+} cations. In the β-form, three of the 5 Si sites are disordered. In Fig. 8, the schematic structure of β-$LaSi_5$ is shown using the centers of the three disordered Si pairs, Si3* for Si3a–Si3b, Si4* for Si4a–Si4b, and Si5* for Si5a–Si5b. The atomic coordinates of the averaged sites are also given in Table 2. The structure of α-$LaSi_5$ is very close to the averaged structure of β-$LaSi_2$; the cell volume of the former crystal is slightly smaller than the latter (Table 1).

According to the Zintl-Klemm formalism, the formal charge can be assigned to each Si site. Most of the Si sites of $LaSi_5$ have sp^3-like hybridization except Si2 site which appears to have sp^2 hybridization. The four-bonded Si-sp^3 site, (Si4, Si4a, Si4b), has a formal charge 0. The three-bonded Si-sp^3 sites with lone pair

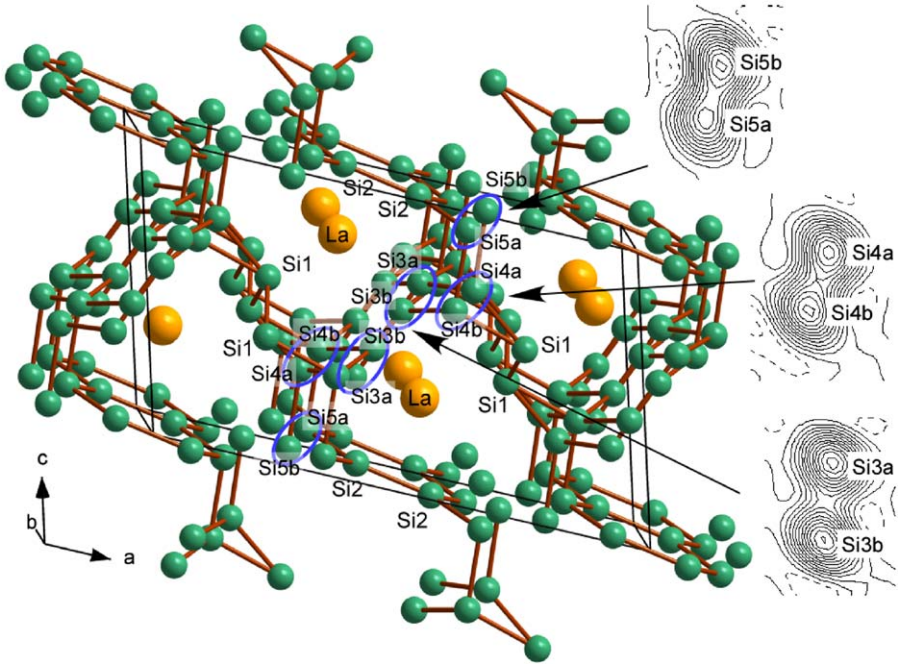

Fig. 7. Schematic illustration of the crystal structure of β-$LaSi_5$. The Fourier maps are corresponding to the three disordered sites.

electrons, Si1, (Si3, Si3a, Si3b) and (Si5, Si5a, Si5b), have a formal charge −1. The Si2 site in almost-planar sp^2 triangle hybridization has a formal charge of 0 with an unhybridized p orbital perpendicular to the plane. Note that the atomic distance Si2–Si2 is 2.39 Å in α- and β-$LaSi_5$ (Table 3), which is a normal Si–Si distance, suggesting that the electrons in the Si2–Si2 unhybridized 3p orbitals do not form localized π-bonds, but are delocalized over the Si network. The delocalization of the electrons from the Si2-3p orbitals would be the reason of the metallic conductivity of $LaSi_5$. The compound can be classified into a Zintl phase with delocalized electrons [31]. In the α-form, the Si3 sites also appears to have sp^2-like coordination rather than sp^3, and again the bond distance 2.39 Å of Si3–Si3 is for a normal Si–Si single bond. The unhybridized p electrons of the Si3 sites could also contribute to the metallic conductivity by delocalization over the silicon covalent network.

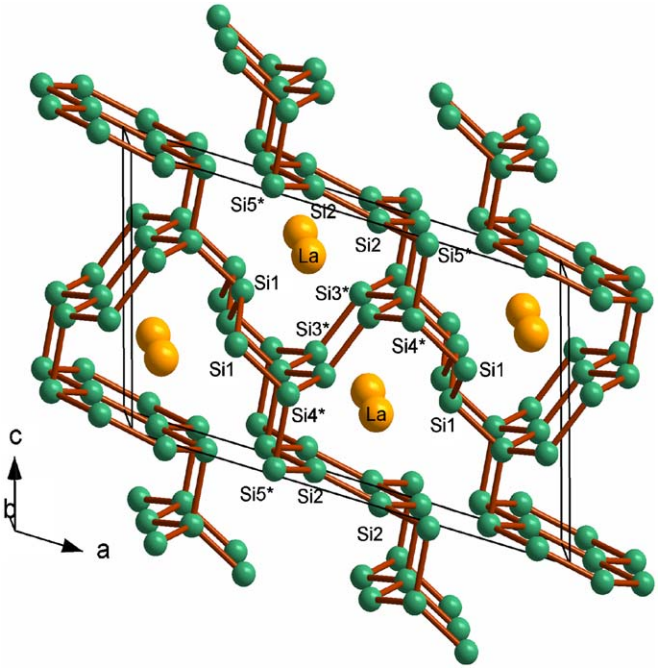

Fig. 8. Schematic illustration of the crystal structure of the averaged β-$LaSi_5$.

In the disordered β-$LaSi_5$, two types of bonding sequences are allowed under a restraint to keep the Si–Si covalent bond lengths at about 2.35 Å apart. The two possible bonding sequences are shown in Fig. 9 and Table 3. Since the site occupation factor of the disordered Si sites are all close to 50% (Fig. 7 and Table 2), the two types of bond sequences should occur in the same probability. At temperatures above 850 °C, $LaSi_5$ should have a totally disordered state with a lattice volume slightly larger than that of the α-form under pressure. When it is cooled down slowly, the Si atoms at the disordered sites try to occupy one of the two sites in each disordered pair. However, all of the Si atoms are covalently bonded in the network. Once one of the sites of a disordered pair is selected, the next linked site is automatically determined, i.e., the disordered Si atoms are not allowed to select their nearest neighbors from the disordered sites randomly. As shown in Table 3 and Fig. 9, for example, if Si5a site is occupied, a stable bonding sequence is (i) Si5a–Si4b–Si3b–Si3a–Si4a–Si5b. If Si5b site is first settled, the other stable sequence is (ii) Si5b–Si4a–Si3a–Si3b–Si4b–Si5a. In other possible bonding sequences, some Si–Si distances between the nearest neighbors are too short or too long for the normal covalent bond formation. Note that both ends of (i) or (ii) sequence given above cannot have the same Si5a or Si5b sites at the same time, i.e., the two sequences must compete against each other. This would retard the transition significantly, and yield a compound with poor crystalline quality.

There is a special situation in this system. The system would be in a totally disordered state at sufficiently high temperatures. As the temperature decreases, the system is going to an ordered state. However, there are two competing ordered states, or two bonding sequences, and as the result the system goes into the second disordered state like β-$LaSi_5$. α-$LaSi_5$ is an ordered form with a structure similar to the averaged β-$LaSi_5$ structure (Fig. 8). The temperature condition seems to be very important for the transformation. If the temperature is too high, the compound has a totally disordered state. On the other hand if temperature is too low, the atomic thermal movement is suppressed under high pressure and Si atoms cannot move between the two disordered sites. The temperature range suitable for the transition should be very narrow, probably in a range from about 850 to 750 °C. If the sample temperature is rapidly cooled down passing through this

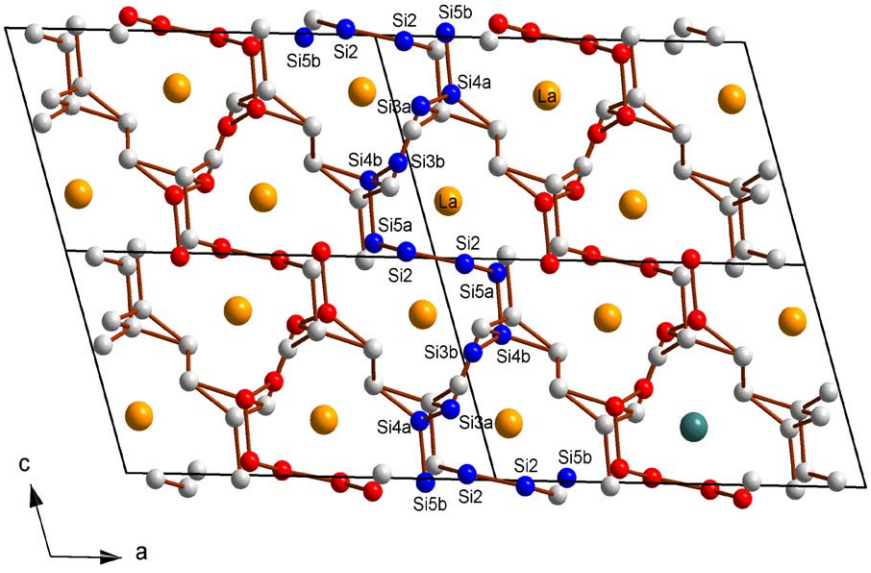

Fig. 9. The disordered structure of β-$LaSi_5$ consisting of two sequences of bonding; (i) Si5b–Si4a–Si3a–Si3b–Si4b–Si5a and (ii) Si5a–Si4b–Si3b–Si3a–Si4a–Si5b.

suitable temperature range in a short time, the crystal remains as the α-form, i.e., an averaged structure form. We tried to prepare the β-form from the α-form using much longer annealing time under high pressure and different temperature conditions. However, samples without the association of the α-form have not been obtained.

Table 4
Atomic coordinates, anisotropic and equivalent displacement parameters (Å^2) for $LaSi_{10}$.

Atom	Position	x	y	z	U_{11}	U_{22}	U_{33}	U_{12}	U_{13}	U_{23}	U_{eq}
La	2*c*	1/3	2/3	1/4	0.028(1)	0.028(1)	0.072(2)	0.014(1)	0	0	0.043(1)
Si1	2*b*	0	0	1/4	0.026(2)	0.026(2)	0.037(3)	0.013(1)	0	0	0.029(2)
Si2	6*h*	0.0457(6)	0.5229(3)	−1/4	0.025(2)	0.028(2)	0.034(2)	0.013(1)	0	0	0.029(1)
Si3	6*h*	0.1850(3)	0.3699(6)	−1/4	0.031(2)	0.031(2)	0.034(2)	0.015(1)	0	0	0.032(1)
Si4	6*h*	0.1429(4)	0.2859(7)	1/4	0.078(3)	0.030(2)	0.031(2)	0.015(1)	0	0	0.052(2)

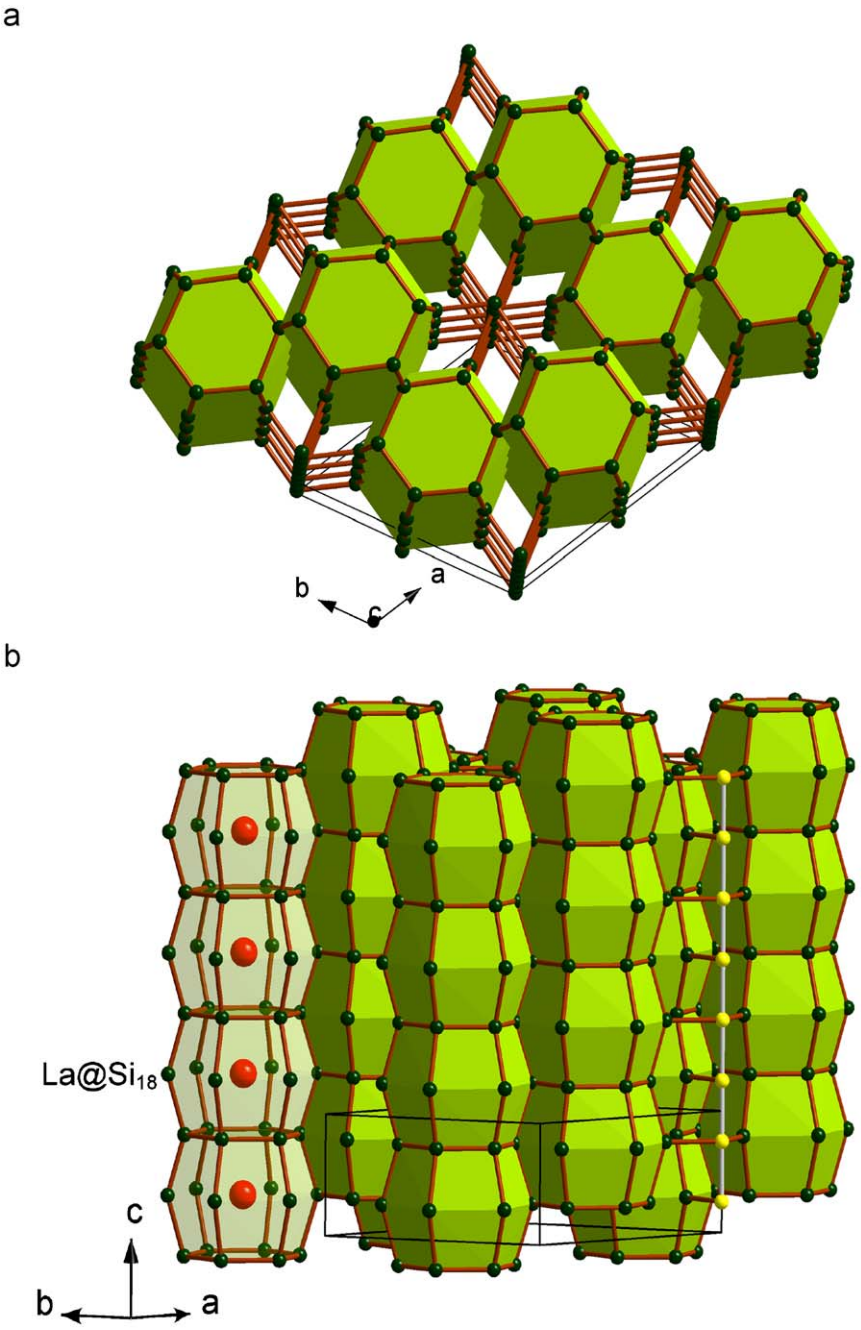

Fig. 10. Schematic structural models of $LaSi_{10}$: (a) the view along the *c*-axis; (b) columnar structure formed by the stacking of La@Si_{18} polyhedra by sharing hexagonal faces. A Si linear chain is highlighted with bright color. (For interpretation of the references to color in this figure legend the reader is referred to the web version of this article.)

As mentioned above, we had α-$LaSi_5$ by heating a molar mixture of $LaSi_2$ and 3 Si at 700 °C. This reaction temperature is not sufficiently high for the thermal motion of Si atoms under high pressure, and thus the compound should have the averaged α-$LaSi_5$ structure. In addition the cell volume of the α-form ($V = 475.7(1)$ Å^3) is slightly smaller than that of the β-form ($V = 490.4(4)$ Å^3), and thus the α-form is more stable under high pressure at low temperatures. It should be noted that the lattice parameters of the α-form have standard deviations one order larger than those of β-$LaSi_5$. This is probably due to the low crystallinity of the average structure. It is reasonable to expect that there would be a continuous parameter change from the values of the α-form to a β-form-like phase. The single crystals of α- and β-forms of the present study must have been formed under a very limited optimum condition.

3.3. *Structure of $LaSi_{10}$ and superconductivity*

Single crystals of another Si-rich binary compound $LaSi_{10}$ were obtained in the study of the phase diagram. The compound became a superconductor with $T_c = 6.7$ K as the magnetic susceptibility measurement showed in Fig. 4(d). The crystallographic data of $LaSi_{10}$ are given in Table 1. The atomic coordinates and thermal parameters are listed in Table 4. A schematic crystal structure of $LaSi_{10}$ is shown in Fig. 10. The compound crystallizes with the space group $6_3/mmc$ and the lattice parameters $a = 9.624(4)$, $c = 4.723(3)$ Å. The structure is composed of La containing silicon polyhedra La@Si_{18} with hexagonal beer barrel shape. The barrels are stacked along the *c*-axis to form straight columns by sharing the flat hexagonal faces. Such one-dimensional columns are bundled side-by-side by sharing side edges as shown in the

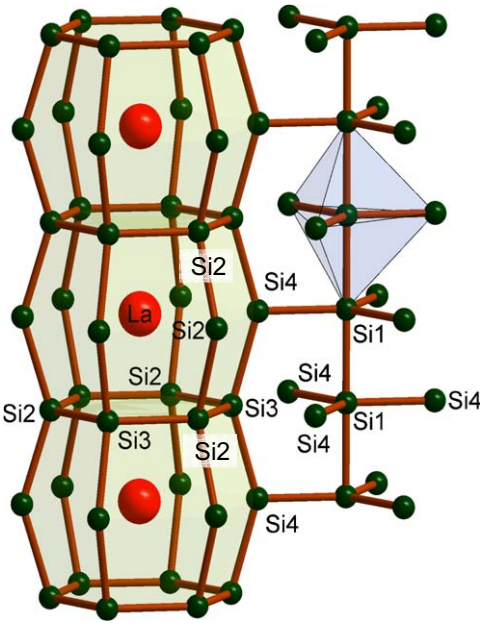

Selected bond distances (Å) and angles of $LaSi_{10}$			
Si1-Si4	2.382(6)	Si1-Si1-Si4	90
Si3-Si4	2.463(3)	Si4-Si1-Si4	120
Si2-Si2	2.481(3)	Si2-Si2-Si2	144.2(4)
Si2-Si3	2.436(4)	Si3-Si2-Si3	123.1(2)
La-Si2	3.159(5)	Si2-Si3-Si2	116.9(2)
La-Si2	3.365(4)	Si2-Si2-Si3	98.41(8)
La-Si3	3.419(4)	Si2-Si3-Si4	98.56(10)
La-Si4	3.174(6)	Si4-Si3-Si4	147.0(4)
Ave (La-Si)	3.279(5)	Si3-Si4-Si3	147.0(4)

Fig. 11. Selected bond distances (Å) and angles of $LaSi_{10}$. The arrangement of the face shared La@Si_{18} polyhedral column and a Si trigonal bipyramid in the linear Si chain are focused.

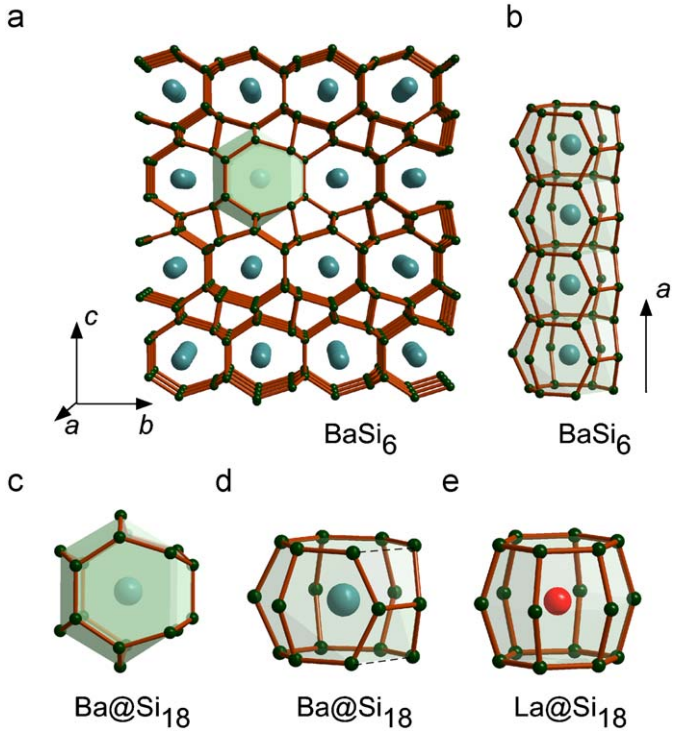

Fig. 12. Schematic structure of $BaSi_6$: (a) the view along the *a* axis; (b) Ba containing column running along the *a* axis; (c) and (d) Ba@Si_{18} polyhedral unit in $BaSi_6$; (e) La@Si_{18} in $LaSi_{10}$.

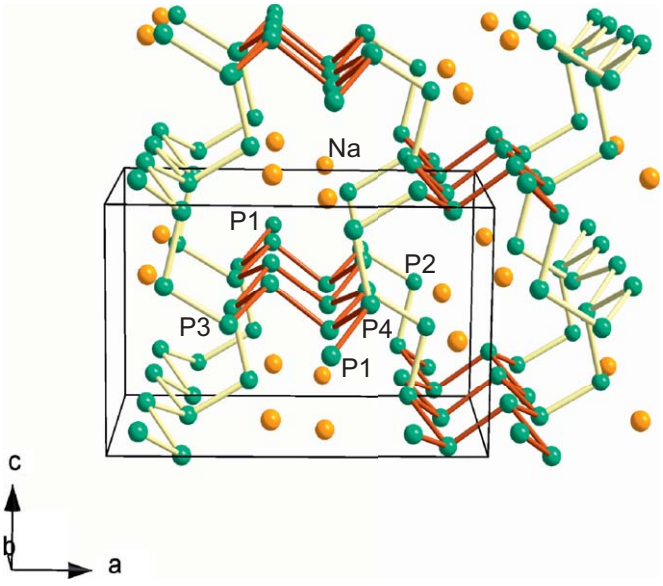

Fig. 13. Schematic illustration of the crystal structure of NaP_5. The six membered P rings with chair conformation are emphasized in dark color. (For interpretation of the references to color in this figure legend the reader is referred to the web version of this article.)

Fig. 10 (b). In the center of the bundle, a straight Si linear chain is running, each Si atom in the chain having trigonal bipyramid five fold coordination. Most of the Si atoms forming La@Si_{18} polyhedra have four fold covalent bonds, however, unlike the Si atoms in Types I and II clathrate structures, the coordination is highly deformed from regular sp^3 hybridization. The selected bond distances and angles are shown in Fig. 11.

We had very similar Si polyhedra in another Si-rich high pressure phase $BaSi_6$ [10]. The structure of $BaSi_6$ is composed of irregular shaped Ba@Si_{18} polyhedra as shown in Fig. 12. The polyhedra are linked by sharing faces to form Ba containing tunnels along the *a* axis. The Ba@Si_{18} polyhedron is considered to have a peculiar irregular shape. However, if we compare it with the polyhedron La@Si_{18}, the two polyhedra resemble each other as shown in Fig. 12 (c)–(e). In Ba@Si_{18} one Si–Si distance (3.62 Å) in the hexagonal plate is longer than the others (~2.4 Å), and thus the bond is open, while the one Si–Si distance (2.42 Å) on the side of the polyhedron is much shorter than the others, having a bond like a waist band of the polyhedron. $BaSi_6$ is isomorphous with $EuGa_2Ge_4$ [11] and the Si-rich high pressure phases $CaSi_6$ and $SrSi_6$ [12,13]. All of the hexasilicides are metallic, but not superconductors.

3.4. Other related compound under high pressure

The crystal structure of $LaSi_5$ can be compared with NaP_5 [32], which is the ordered LiP_5 [33] structure. As shown in Fig. 13, the structure of NaP_5 consists of six membered P rings with chair conformation, which share the P–P edges in a side-by-side manner to form one dimensional ladders running along the *b* direction. The ladders are linked by additional phosphorus atoms (*P*2 in Fig. 13) to form 18 membered phosphorus rings; Na^+ cations resides in the open channels made of the 18 membered rings. The α-$LaSi_5$ structure contains two types of six membered Si rings composed of [2 Si5+4 Si2] and [2 Si4+4 Si3], which have more or less coplanar chair conformations as shown in Fig. 14. The coplanar six membered rings form one-dimensional Si ladders,

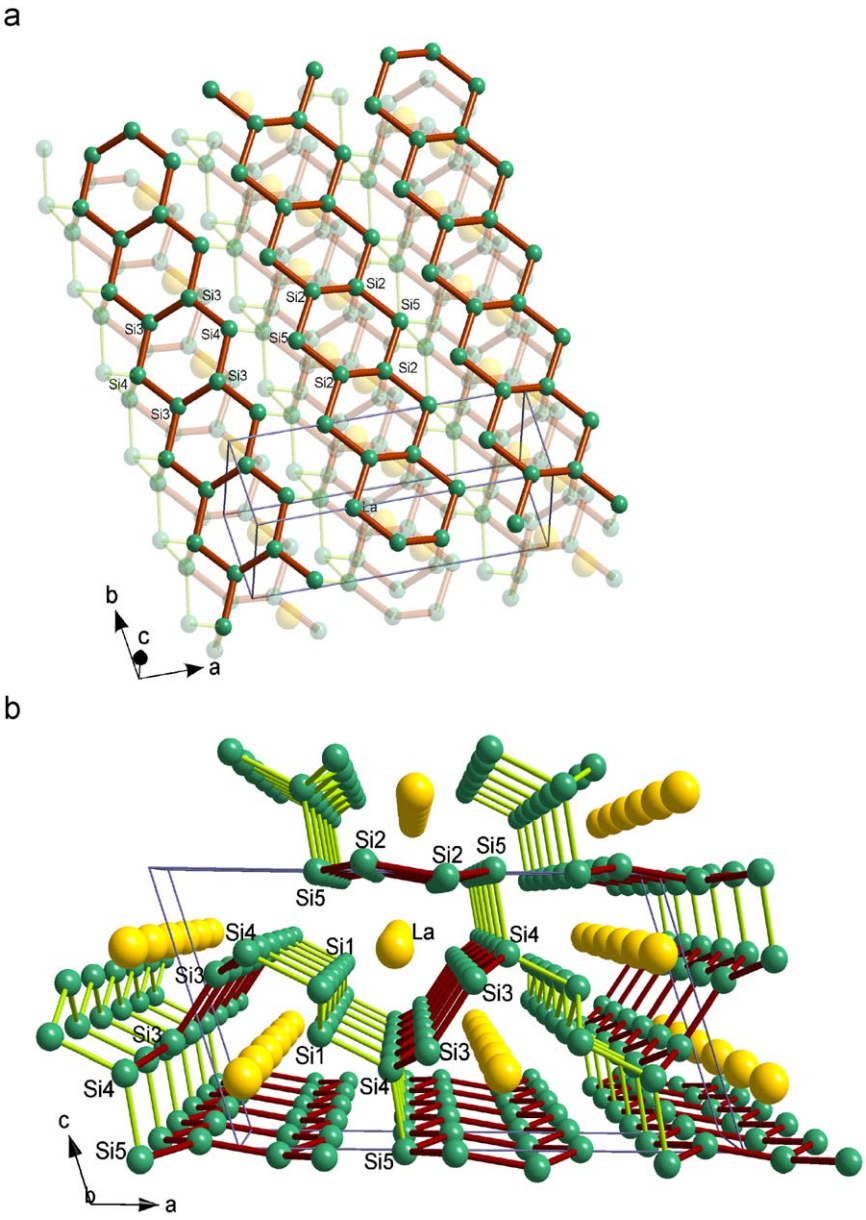

Fig. 14. Sila-polyacene ribbons included in α-$LaSi_5$: (a) the top view from the *c* axis; (b) the side view through the *b* axis.

or sila-polyacene ribbons as depicted in Fig. 14a. The Si2 and Si3 atoms having sp^2 hybridization have unhybridized p electrons, which will be delocalized over the sila-polyacene ribbons for superconductivity. Such ribbons are directly bonded to the neighboring ribbons located above and below at the Si4–Si5 sites to form the folded structure along the c axis. The folded ladders are linked together with the additional –Si1–Si1– zig-zag chains to form the three dimensional structure.

In a previous study [14], the Ge rich binary compound $LaGe_5$ was prepared under pressure of 5 GPa at 1200 °C. As shown in Fig. 15, the structure is very different from that of $LaSi_5$. The structure also consists of six membered Ge rings but with all boat conformation. This is a Zintl compound with the formal charge, $[La^{3+}Ge2^{+}]\ {}^{2}_{\infty}[GeI_4]^{-4}$; 4 Ge1 sites have sp^3 hybridization with a lone pair, and the six membered Ge rings with all boat conformation are linked two-dimensionally. $Ge2^{+}$ and La^{3+} cations are located between the two dimensional network. The $Ge2^{+}$ is coordinated by eight lone pairs. The structure can be seen as a tunnel network with La^{3+} ions in the channels. It is interesting to note that $LaSi_5$ and $LaGe_5$ have very different structures, irrespective of the lanthanides of the same 14 group elements in the periodic table and the same atomic ratio. $LaGe_5$ is also a superconductor with $Tc = 7.0$ K [14].

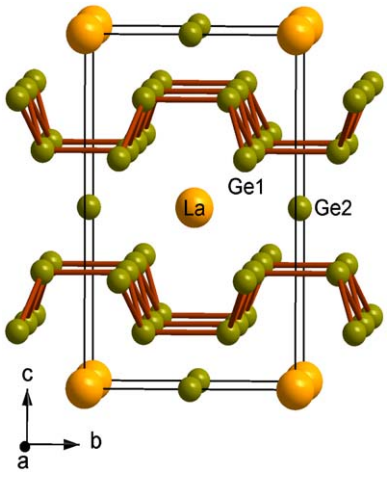

Fig. 15. The structure of $LaGe_5$ consisting of six membered Ge rings in all boat conformation.

3.5. *Ab initio calculation*

The two silicon-rich compounds, α-$LaSi_5$ and $LaSi_{10}$, were geometrically optimized including lattice parameters and the coordinates by the *ab initio* calculation software CASTEP. The results are compared in Table 5. As can be seen from the table, the X-ray refined and the *ab initio* optimized crystallographic data agree very well. The density of states (DOS) were calculated on the two structures based on the optimized structures, and are shown in Fig. 16. Both DOS profiles resemble very much and have large density of states at the Fermi level. The DOS near the Fermi level are composed of Si-3p orbitals and a small contribution of La-5d orbital. As mentioned in the formal charge assignment in α-$LaSi_5$, Si2 and Si3 sites have sp^2 hybridization with one electron in each unhybridized 3p orbital, which will be delocalized over the covalent network. Although more detailed theoretical study is needed, it is likely that these p electrons can contribute to the conduction electrons near the Fermi level.

4. Conclusions

In the study of the La–Si binary phase diagram under a pressure of 13.5 GPa, two new Si-rich compounds $LaSi_5$ and $LaSi_{10}$ have been prepared, which have peritectic decomposition

Table 5
Crystallographic data for α-$LaSi_5$ and $LaSi_{10}$ determined by X-ray structural analysis in comparison with the structural data optimized by CASTEP. The geometry optimization includes the lattice parameters and the coordinates.

α-$LaSi_5$							
	X-ray refinement (space group $C2/m$)				Geometry optimized (CASTEP)		
a (Å)	15.11(3)				15.1326		
b (Å)	4.032(6)				4.0635		
c (Å)	8.26(1)				8.3010		
β (°)	109.11(1)				108.25		
Atom	Position	x	y	z	x	y	z
La	4*i*	0.4319(1)	0	−0.2777(2)	0.42906	0	−0.27446
Si1	4*i*	0.2308(4)	0	0.4142(8)	0.23179	0	0.41804
Si2	4*i*	0.4256(4)	1/2	0.0248(9)	0.42569	1/2	0.02587
Si3	4*i*	0.4353(5)	1/2	0.3777(10)	0.43604	1/2	0.37414
Si4	4*i*	0.3487(5)	0	0.2907(9)	0.35117	0	0.29482
Si5	4*i*	0.3253(4)	0	−0.0070(9)	0.32145	0	−0.00165
$LaSi_{10}$							
	X-ray refinement (space group $P6_3/mmc$)				Geometry optimized (CASTEP)		
a (Å)	9.623(4)				9.626472		
c (Å)	4.723(1)				4.773979		
Atom	Position	x	y	z	x	y	z
La	2*c*	1/3	2/3	1/4	1/3	2/3	1/4
Si1	2*b*	0	0	1/4	0	0	1/4
Si2	6*h*	0.0457(6)	0.5229(3)	−1/4	0.047157	0.523579	−1/4
Si3	6*h*	0.1850(3)	0.3699(6)	−1/4	0.182267	0.364534	−1/4
Si4	6*h*	0.1429(4)	0.2859(7)	1/4	0.142401	0.284801	1/4

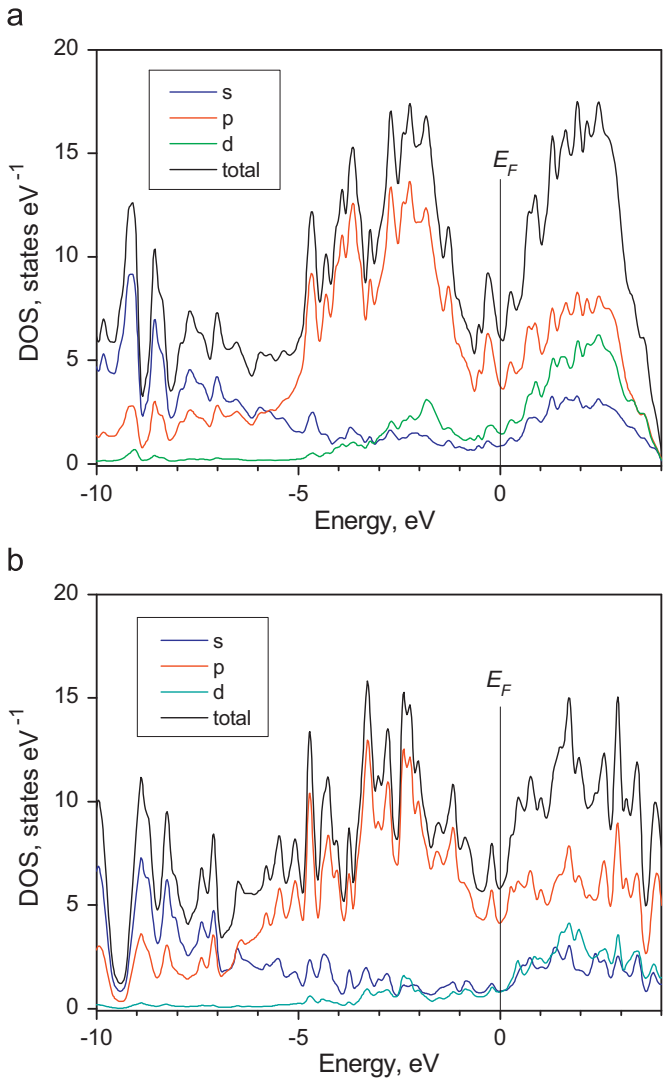

Fig. 16. DOS profiles of α-$LaSi_5$ and $LaSi_{10}$ calculated by CASTEP.

temperatures at 980 and 750 °C, respectively. The single crystal X-ray studies revealed that there are two polymorphs α- and β-$LaSi_5$ with averaged and disordered Si network structures, respectively. The β-form is formed in the incomplete transformation of the α-form on cooling. The formal charges can be assigned to both polymorphs according to Zintl formalism with delocalized electrons. The structures contain unique one-dimensional sila-polyacene ribbons. α-$LaSi_5$ is a superconductor with $T_c = 11.5$ K, while the β-form is metallic but not superconducting. The structure of $LaSi_5$ is very different from $LaGe_5$. The other Si-rich binary phase $LaSi_{10}$ is composed of La@Si_{18} polyhedra with beer barrel shape, which form straight columns by stacking along the *c*-axis via face sharing. One-dimensional columns of La@Si_{18} barrels are edge-shared, and bundled with infinite Si trigonal bipyramid chains via corner sharing. $LaSi_{10}$ shows superconductivity with $T_c = 6.7$ K. It is interesting to note that the shape of polyhedral unit La@Si_{18} has a close relation with that of Ba@Si_{18} found in $BaSi_6$ high pressure phase. It is also established that high pressure and high temperature condition is favorable for the formation of Si-rich compounds in La–Si binary system as well as in the Ba–Si binary system.

Acknowledgments

This study has also been supported by a Grant-in-Aid for Scientific Research (Grants 19105006, 19051011, and 19014016) of the Ministry of Education, Culture, Sports, Science, and Technology of Japan.

Appendix A. Supplementary material

Supplementary data associated with this article can be found in the online version at doi:10.1016/j.jssc.2009.05.010.

References

[1] J. Evers, J. Solid State Chem. 32 (1980) 77.
[2] M. Imai, T. Hirano, Phys. Rev. B 58 (1998) 11922.
[3] M. Imai, T. Kikegawa, Chem. Mater. 15 (2003) 2543.
[4] H. Nakano, S. Yamanaka, J. Solid State Chem. 108 (1994) 266.
[5] J. Evers, G. Oehlinger, A. Weiss, J. Solid State Chem. 20 (1977) 173.
[6] H. Fukuoka, K. Ueno, S. Yamanaka, J. Organomet. Chem. 611 (2000) 543.
[7] S. Yamanaka, E. Enishi, H. Fukuoka, M. Yasukawa, Inorg. Chem. 39 (2000) 56.
[8] S. Yamanaka, H. Kawaji, M. Ishikawa, Material science forum, in: K. Sattler (Ed.), Cluster Assembled Materials, vol. 232, 1996, 103.
[9] T. Rachi, H. Yoshino, R. Kumashiro, M. Kitajima, K. Kobayashi, K. Yokogawa, K. Murata, N. Kimura, H. Aoki, H. Fukuoka, S. Yamanaka, H. Shimotani, T. Takenobu, Y. Iwasa, T. Sasaki, N. Kobayashi, Y. Miyazaki, K. Saito, F. Guo, K. Kobayashi, K. Osaka, K. Kato, M. Takata, K. Tanigakil, Phys. Rev. B 72 (2005) 144504.
[10] S. Yamanaka, S. Maekawa, Z. Naturforsch. 61b (2006) 1493.
[11] W. Carrillo-Cabrera, S. Paschen, Y. Grin, J. Alloys Compd. 333 (2002) 4.
[12] A. Wosylus, Y. Prots, U. Burkhardt, W. Schnelle, U. Schwarz, Y. Grin, Z. Naturforsch. B 61 (2006) 1485.
[13] A. Wosylus, Y. Prots, U. Burkhardt, W. Schnelle, U. Schwarz, Sci. Tech. Adv. Mater. 8 (2007) 383.
[14] H. Fukoka, S. Yamanaka, Phys. Rev. B 67 (2003) 094501.
[15] H. Fukuoka, S. Yamanaka, E. Matsuoka, T. Takabatake, Inorg. Chem. 44 (2005) 1460.
[16] D. Gout, E. Benbow, G.J. Miller, J. Alloys Compd. 338 (2002) 153.
[17] E.I. Gladyshevskii, Izvestiya Akad. Nauk SSSR, Neorganicheskie Materialy 1 (1965) 648.
[18] H.F. Yang, G.-H. Rao, W.G. Chu, G.Y. Liu, Z.W. Ouyang, J.K. Liang, J. Alloys Compd. 334 (2002) 131.
[19] A. Gaman, H. Steinfink, Acta Crystal 22 (1967) 688.
[20] H.J. Mattausch, O. Oeckler, A. Simon, Z. Anorg. Allg. Chem. 625 (1999) 1151.
[21] N. Kawai, S. Endo, Rev. Sci. Instrum. 41 (1970) 1178.
[22] G.M. Sheldrick, Computer code SHELX97, Program for Structure Refinement, University of Gottingen, Germany, 1997.
[23] L.J. Farrugia, J. Appl. Crystallogr. 32 (1999) 837.
[24] A. Coelho, TOPAS—Academic v 4.1: general profile and structure analysis software for powder diffraction data, Brisbane, 2007.
[25] CASTEP is available from Accelrys, San Diego, CA, 〈 http://www.accelrys.-com〉.
[26] M.D. Segall, P.J.D. Lindan, M.J. Probert, C.J. Pickard, P.J. Hasnip, S.J. Clark, M.C. Payne, J. Phys Condens. Matter 14 (2002) 2717.
[27] I. Binder, J. Am. Ceram. Soc. 43 (1960) 287.
[28] J. Emsley, The Elements, Oxford University Press, Oxford, 1998.
[29] W.E. Henry, C. Betz, H. Muir, Bull. Am. Phys. Soc. 7 (1962) 474.
[30] H. Nakano, S. Yamanaka, J. Solid State Chem. 108 (1994) 260.
[31] R. Nesper, Prog. Solid State Chem. 20 (1990) 1.
[32] X. Chen, S. Yamanaka, J. Alloys Comp. 370 (2004) 110.
[33] H.G. von Schnering, W. Wichelhaus, Naturwissenschaften 59 (1972) 78.